Supporting Information

Scalable Fabrication of Large-area Lithium/Graphene Anode towards Long-life 350 Wh kg^{-1} Lithium Metal Pouch Cell

Bangyi He [a, c, #], *Wei Deng* [a, #], *Qigao Han* [a], *Wenhua Zhu* [a], *Zhiyuan Hu* [a], *Wei Fang* [a], *Xufeng Zhou* [*, a, b] *and Zhaoping Liu* [*, a, b]

a Key Laboratory of Graphene Technologies and Applications of Zhejiang Province and Advanced Li-ion Battery Engineering Laboratory of Zhejiang Province, Ningbo Institute of Materials Technology & Engineering, Chinese Academy of Sciences, Zhejiang 315201, P. R. China

b Center of Materials Science and Optoelectronics Engineering, University of Chinese Academy of Sciences, Beijing 100049, P. R. China

c Department of Materials Science and Engineering, Shanghai University, Shanghai 200444, P. R. China

# These authors contribute equally to this work.

* Corresponding authors. Tel./Fax: +86-574-8668-5096.

E-mail address: zhouxf@nimte.ac.cn, liuzp@nimte.ac.cn

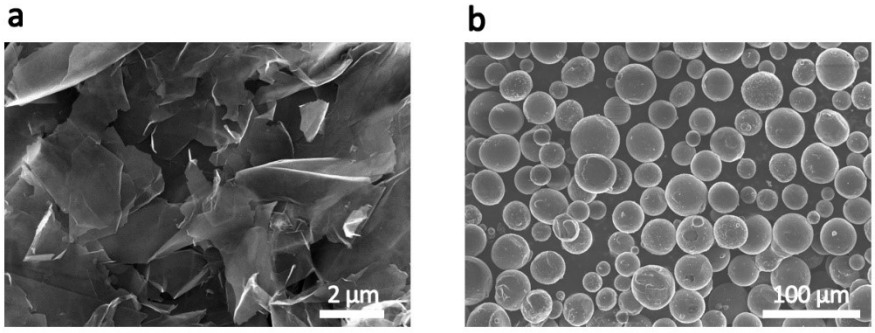

Figure S1. SEM images of (a) graphene flakes and (b) lithium powders.

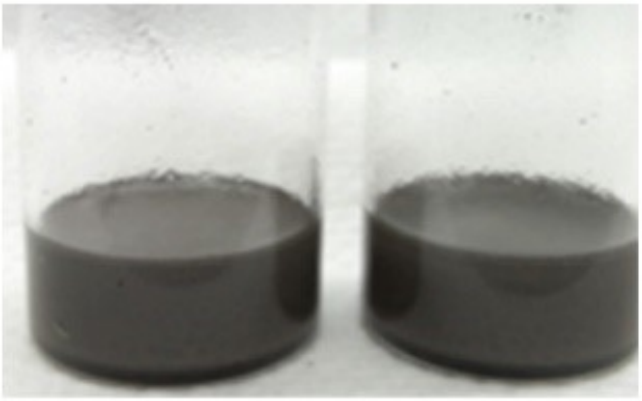

Figure S2. Optical photograph of LP/G/PVDF/NMP slurry.

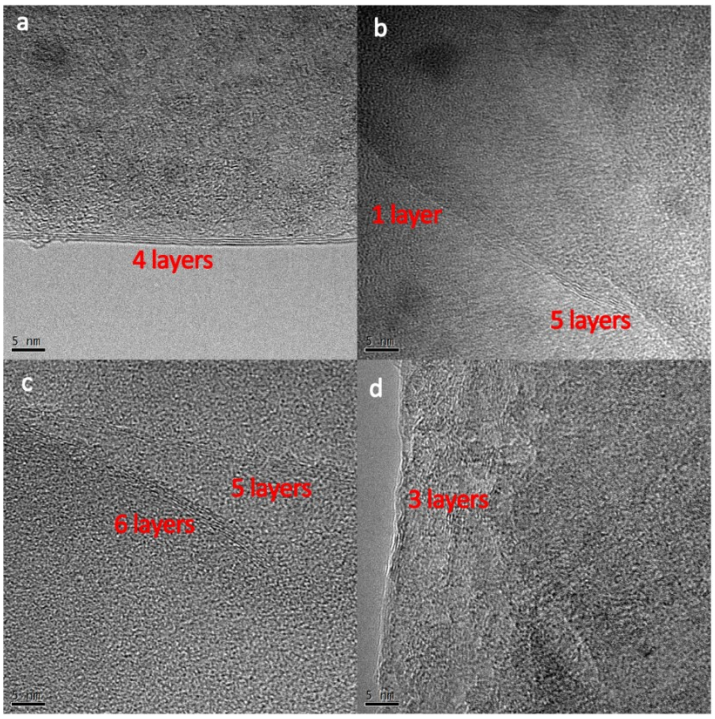

Figure S3. TEM images of multi-layer graphene sample used in our experiment.

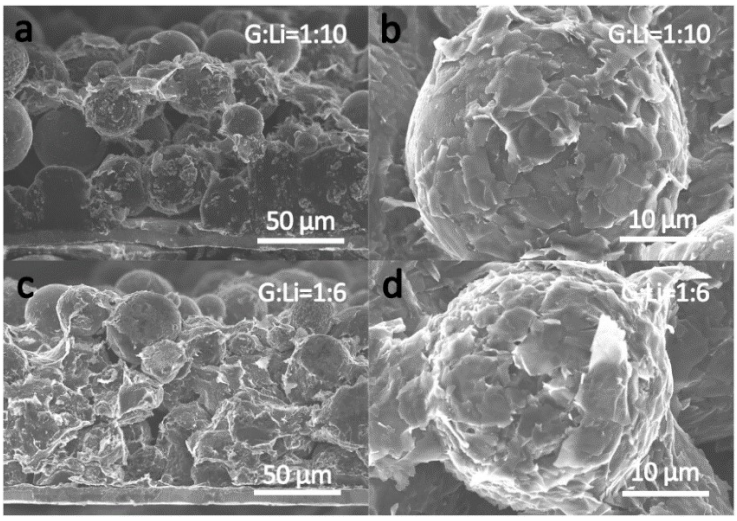

Figure S4. SEM images of the morphology of the Li/G composite before thermal conversion with different graphene to lithium mass ratios of 1:10 (a, b) and 1:6 (c, d).

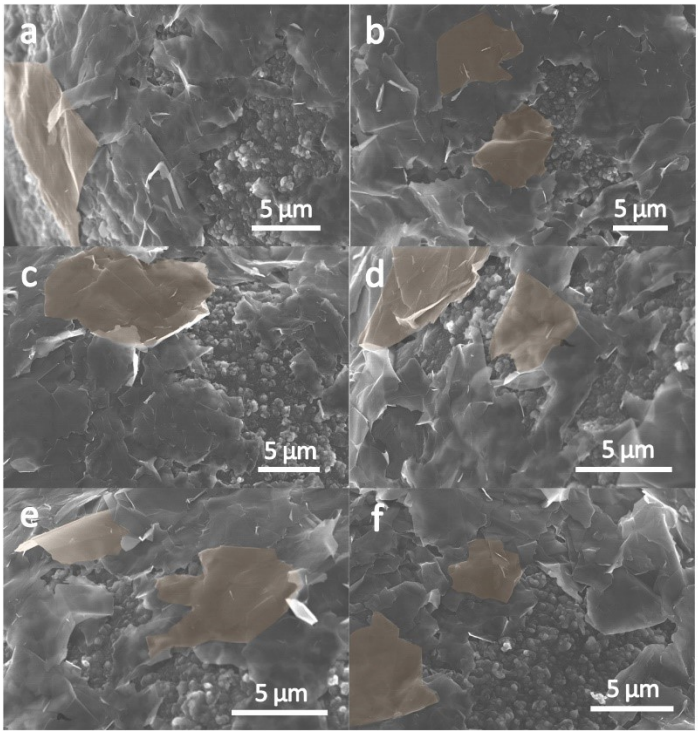

Figure S5. Magnified SEM image of graphene wrapped Li powder in the Li/G composite with the graphene to lithium mass ratio of 1:8.

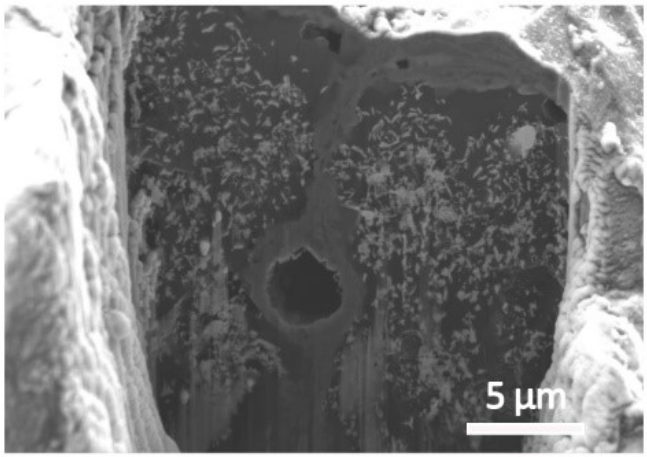

Figure S6. Original SEM image of Figure 1j.

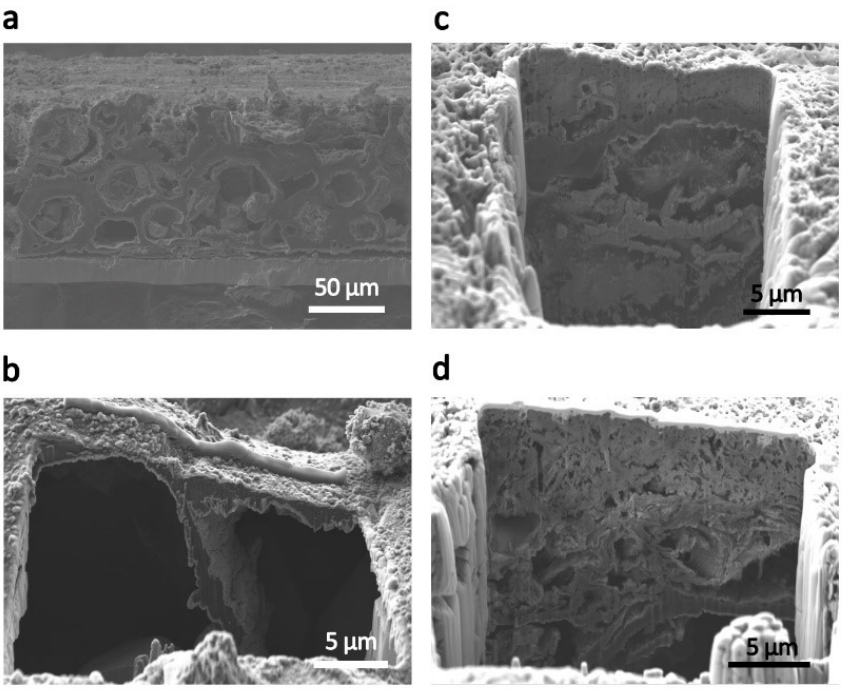

Figure S7. Original SEM images of Figure 2a-d.

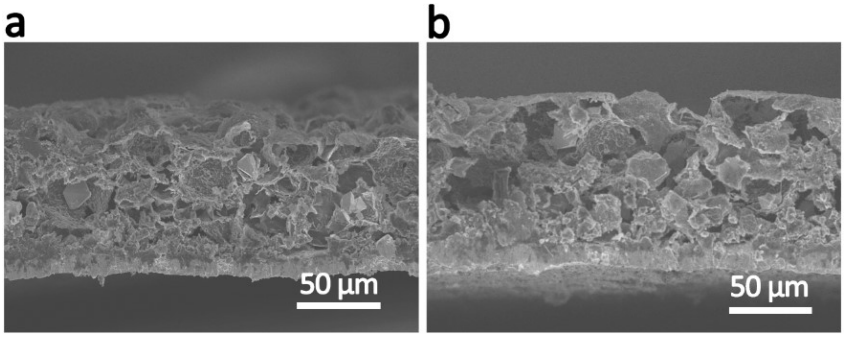

Figure S8. (a, b) Cross-sectional SEM image of the LiC_6 skeleton in the Li@G anode after removal of lithium metal.

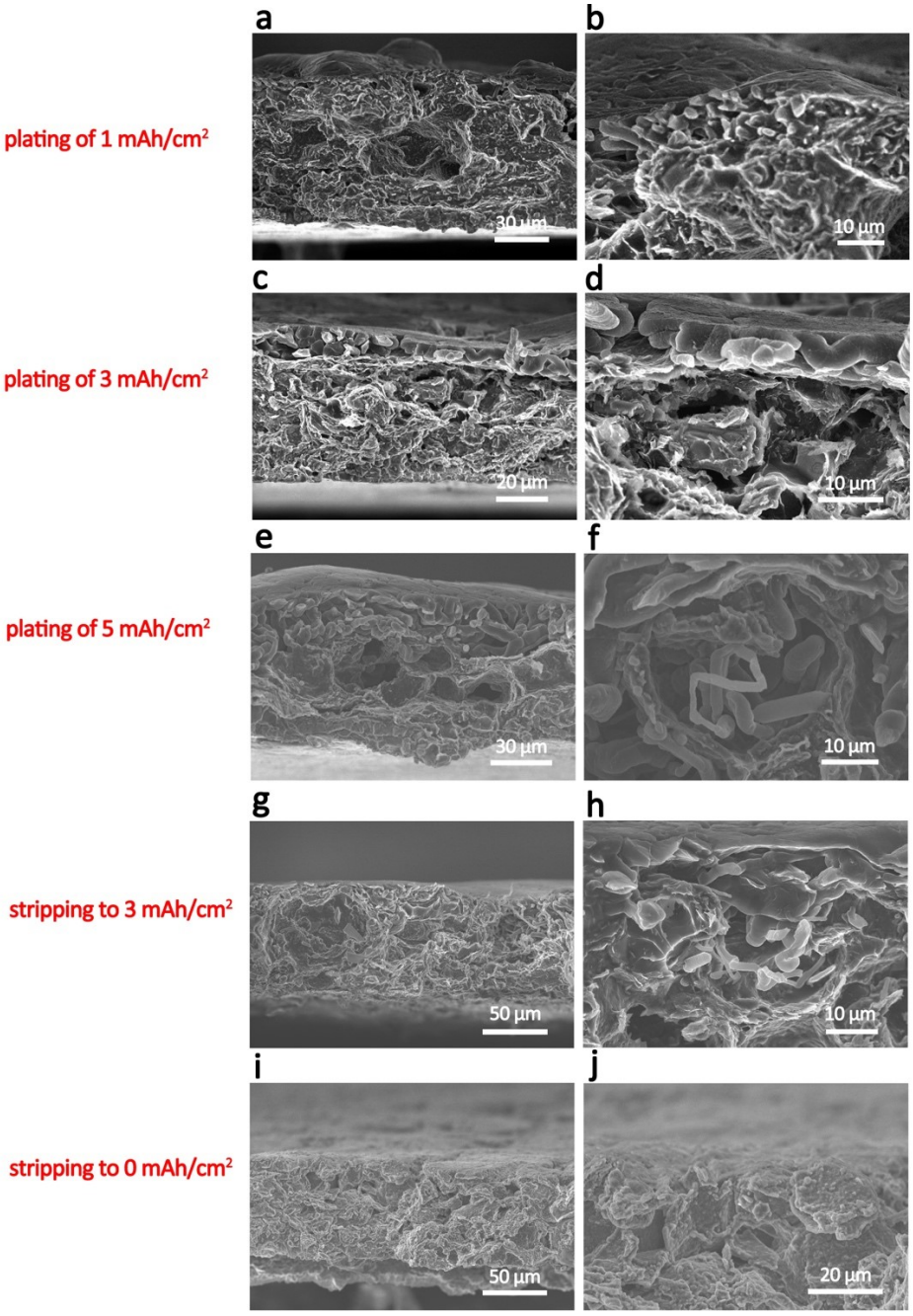

Figure S9. SEM images of Li@G anode with Li plating capacity of (a, b) 1 mAh cm^{-2}, (c, d) 3 mAh cm^{-2} and (e, f) 5 mAh cm^{-2}. SEM images of Li@G anode when stripped with a capacity of (g, h) 2 mAh cm^{-2} and (i, j) 5 mAh cm^{-2}.

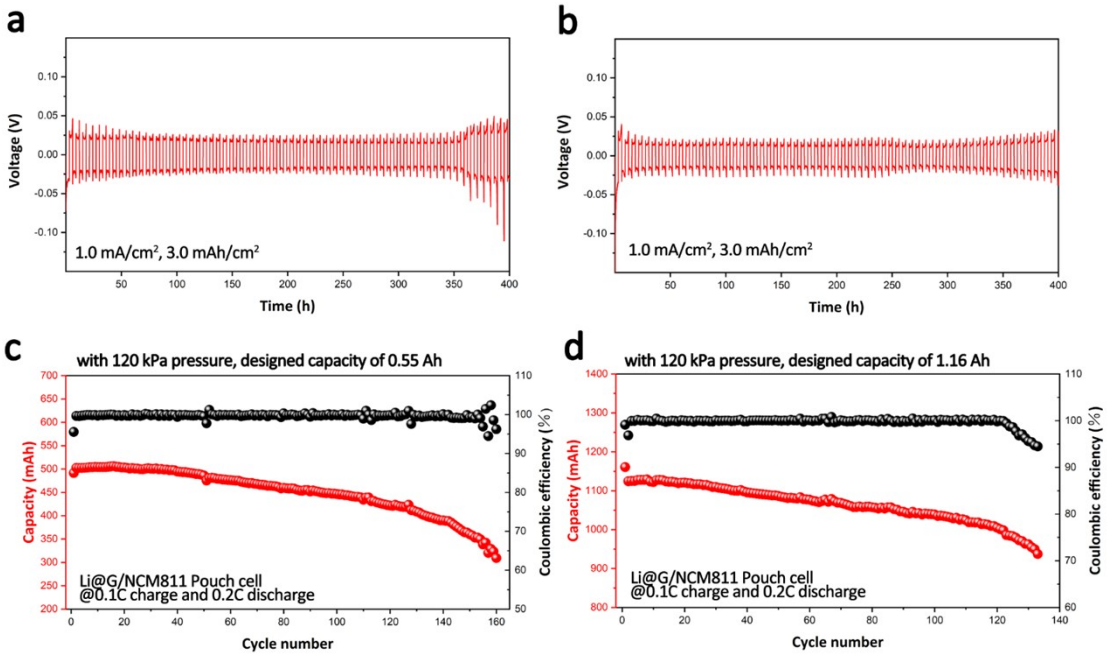

Figure S10. (a, b) Galvanostatic cycling performances of symmetric cells using the Li@G electrodes at a current density of 1.0 mA/cm^2 and a stripping/plating capacity of 3.0 mAh/cm^2. Discharge capacity and Coulombic efficiency of (c) 0.55 Ah and (d) 1.16 Ah pouch cells using Li@G anodes at 0.1 C charge rate and 0.2 C discharge rate.

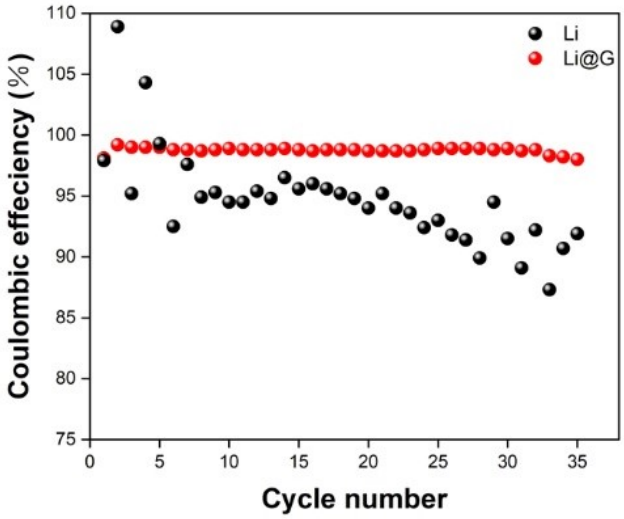

Figure S11. CE of Li-Cu half cells by using Li foil and Li@G as counter electrodes at a current density of 1.0 mA/cm^2 with an areal capacity of 3.0 mAh/cm^2.

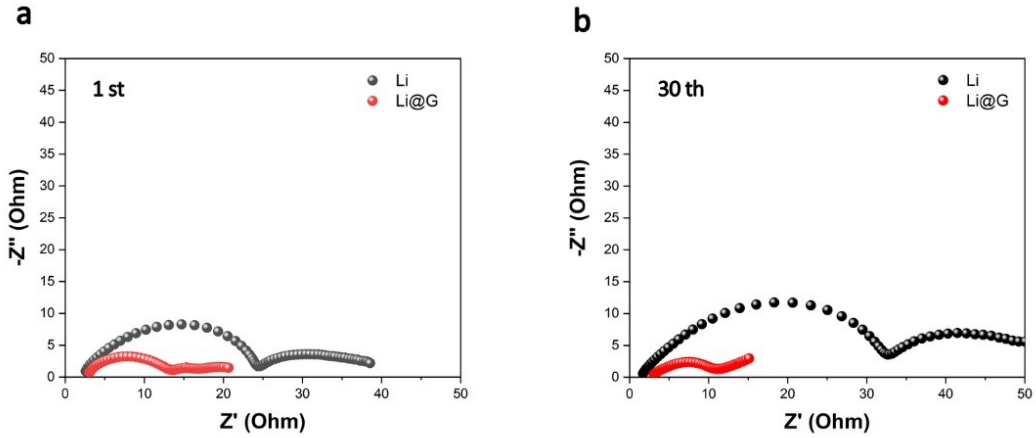

Figure S12. Nyquist plots for Li foil and Li@G symmetric cells (a) after the first cycle and (b) after 30 cycles.

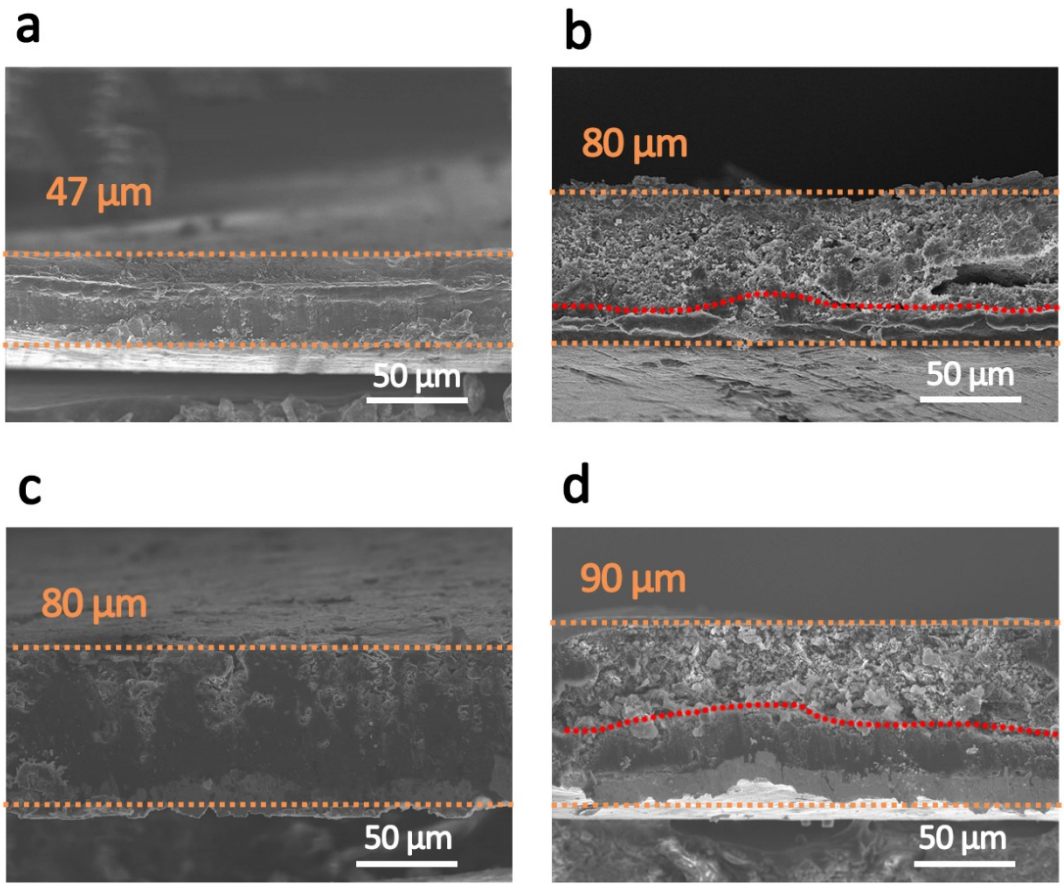

Figure S13. Cross-sectional SEM images of (a) pristine Li foil and (b) Li foil after 30 cycles in symmetric cells tested under an areal capacity of 3.0 mAh/cm^2. Cross-sectional SEM images of (c) pristine Li@G anode and (d) Li@G anode after 30 cycles in symmetric cells tested under an areal capacity of 3.0 mAh/cm^2.

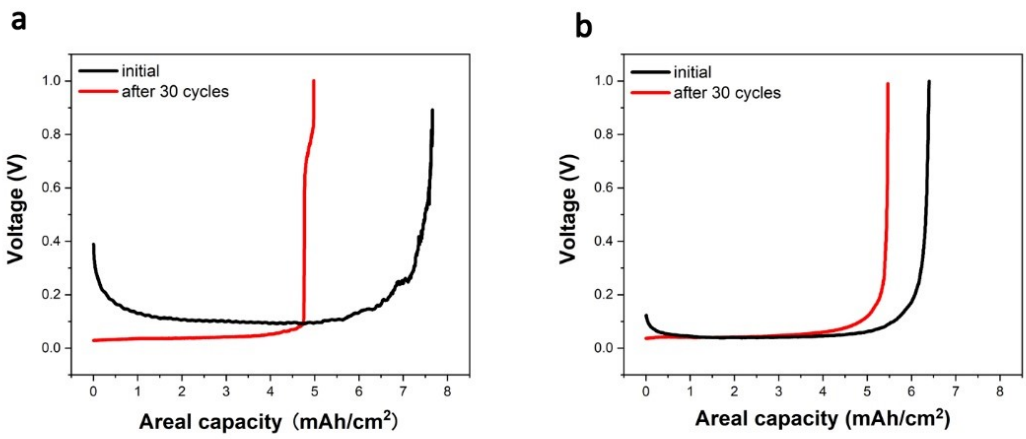

Figure S14. Electrochemical stripping curves of (a) Li foil and (b) Li@G electrode before and after 30 cycles at a current density of 1.0 mA/cm^2 with an areal capcity of 3.0 mAh/cm^2.

Figure S15. Optical photograph of the planetary rotary homogenizer.

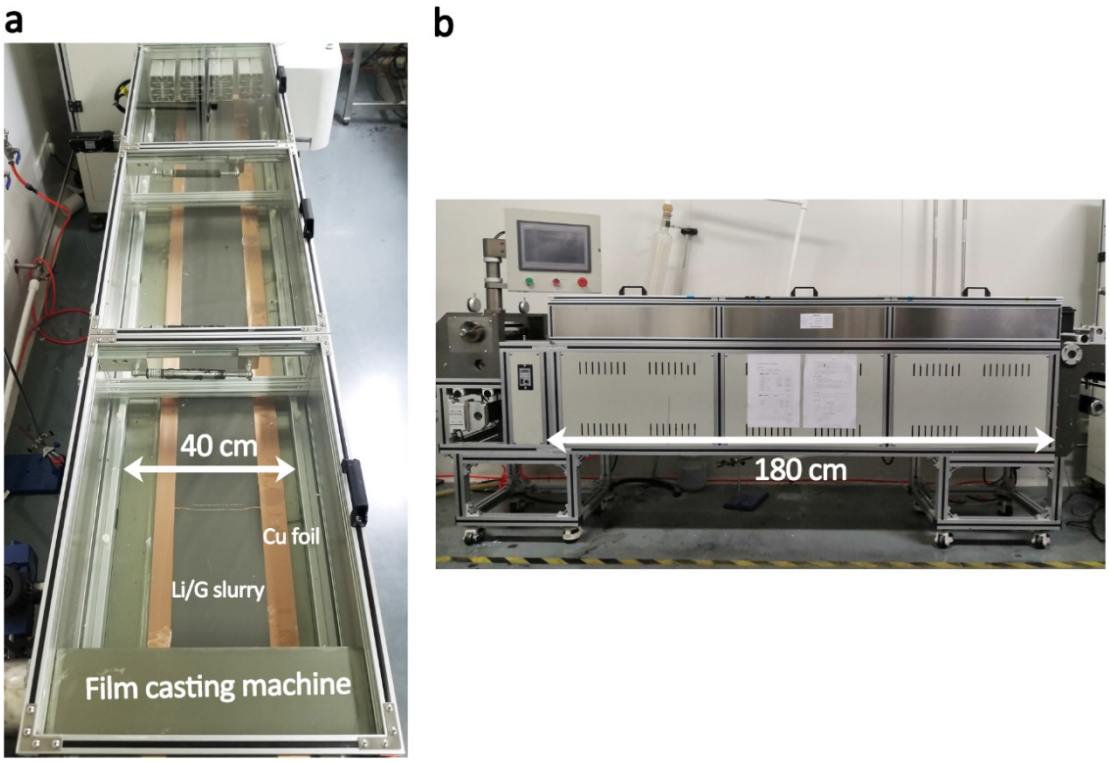

Figure S16. Photographs showing continuous casting of Li/G slurry using a coating-drying machine for the roll-to-roll preparation of Li/G foils.

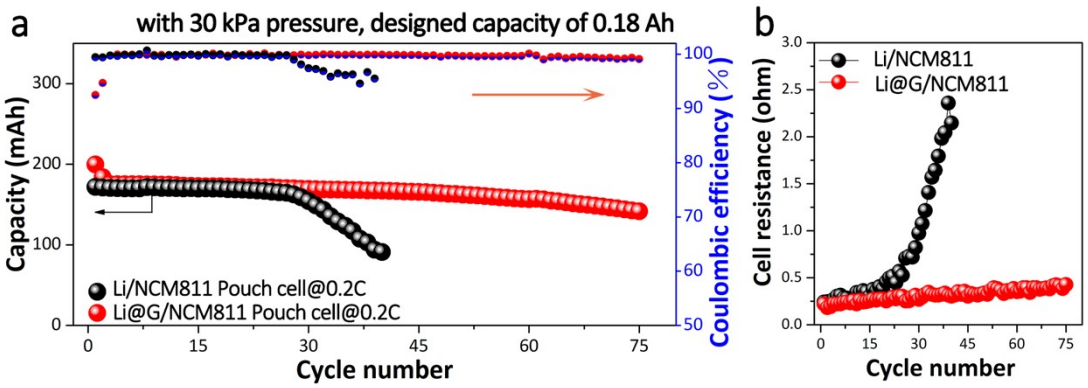

Figure S17. (a) Discharge capacity, Coulombic efficiency and (b) discharge cell resistance of 0.18 Ah pouch cells using Li@G anode and bare Li foil anode at 0.2 C rate.

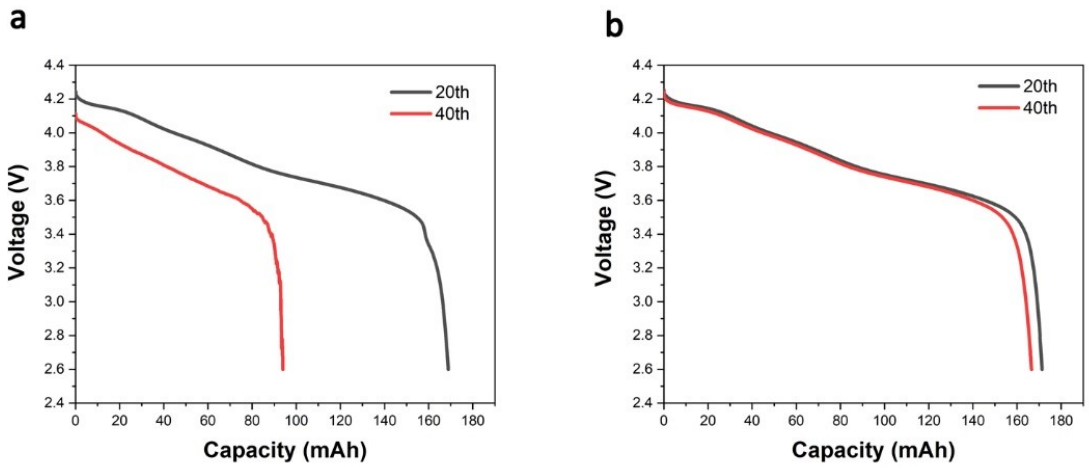

Figure S18. Discharge curves of (a) Li/NCM811 pouch cell and (b) Li@G/NCM811 pouch cell at the 20th cycle and the 40th cycle.

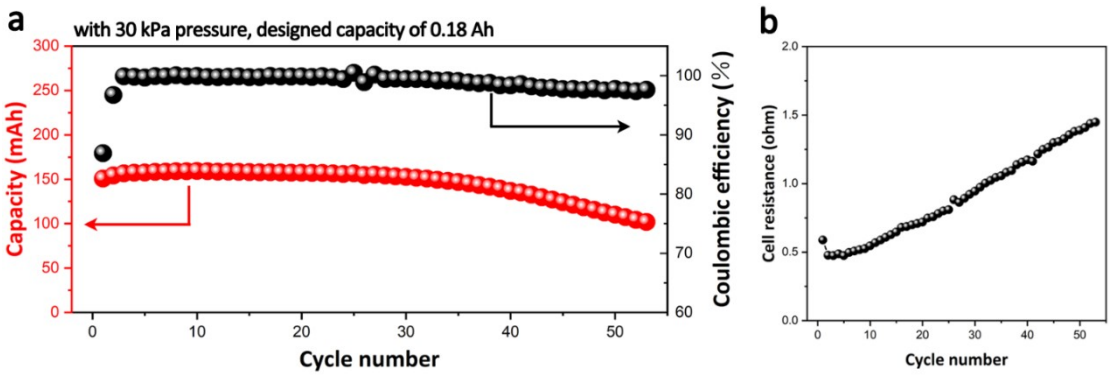

Figure S19. (a) Discharge capacity and Coulombic efficiency, and (b) discharge cell resistance of commercial Li metal laminated on Cu foil at rate of 0.2 C in 0.2 Ah Li@Cu/NCM811 pouch cell.

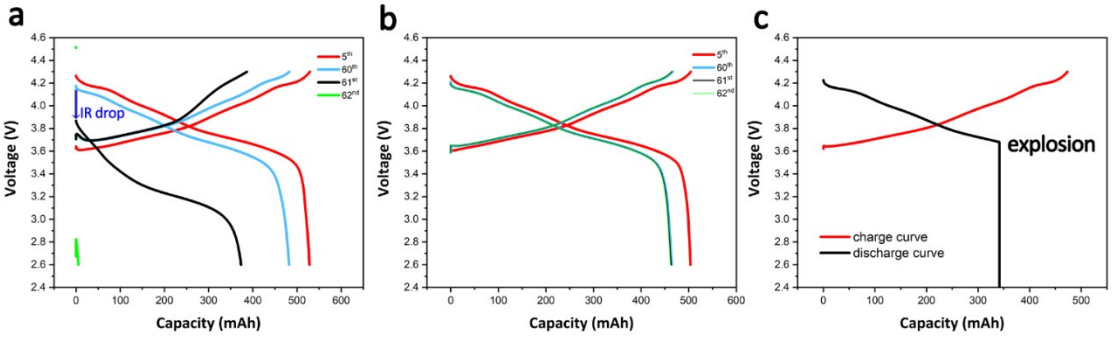

Figure S20. Charge and discharge curves of (a) Li/NCM811 pouch cell and (b) Li@G/NCM811 pouch cell at the 5th, 60th, 61st and 62nd cycle. (c) Typical charge and discharge curves of short circuit cells. During practical testing, the shorting of cell will cause sudden drop of voltage to zero and may result in explosion of lithium metal pouch cells, which is not observed in our experiments (Figure S20c). Moreover, the data of cell resistance and the variation of pressure curves in the main text and supporting information firmly manifest that "dead Li" layer is the main cause of the cell failure.

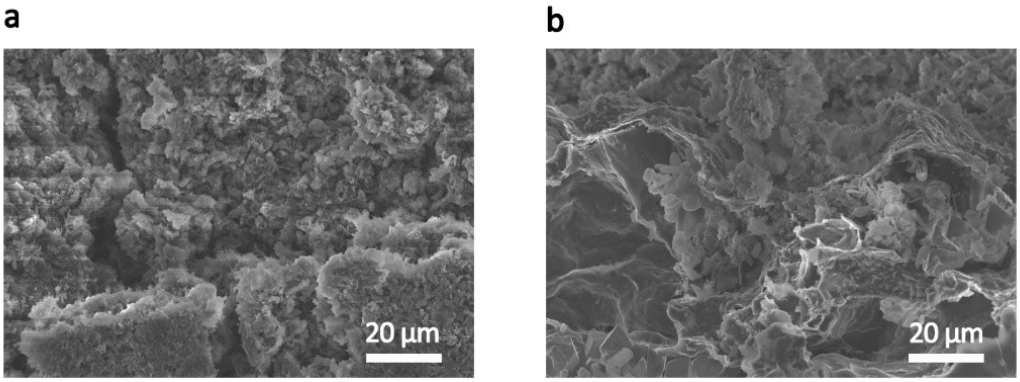

Figure S21. Magnified SEM images of (a) "dead Li" and (b) "dead Li" contacting with the LiC_6 skeleton in the Li@G anode.

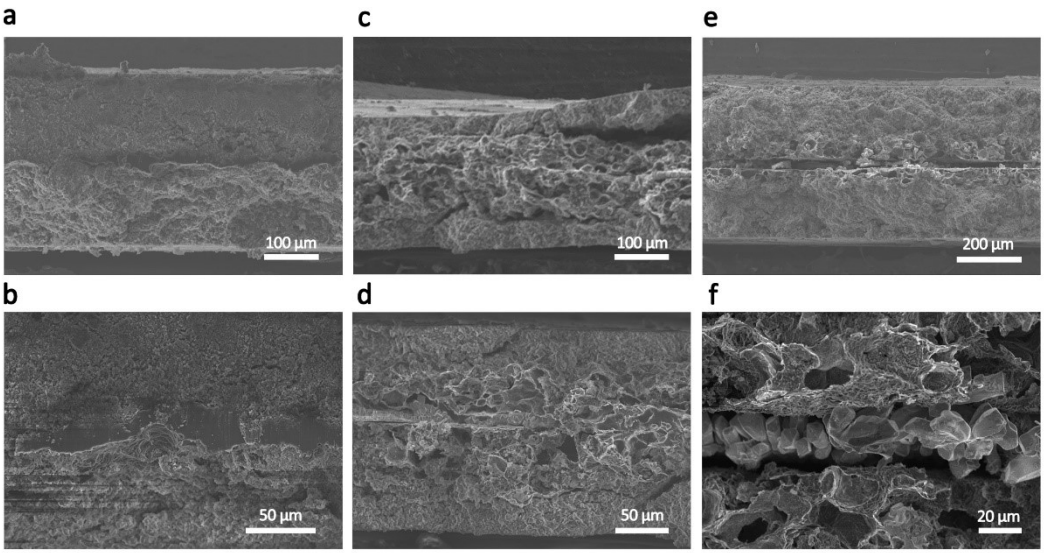

Figure S22. Original SEM images of Figure 5b-c, e-f, h-i.

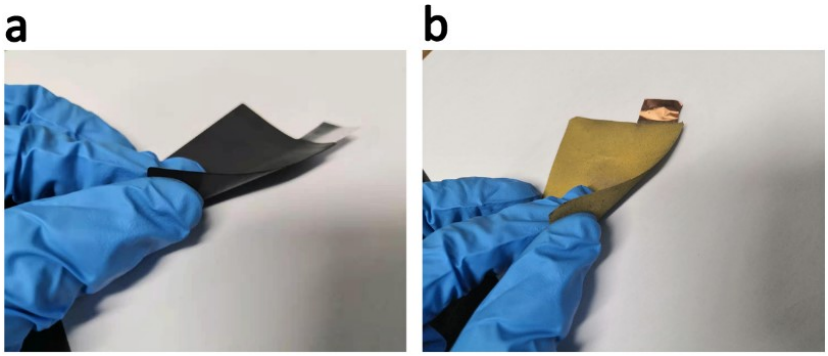

Figure S23. Digital hotographs of the cathode (a) and anode with active materials on double sides.

Table S1. The comparison on vital parameters of Li metal cells in this work and previously reported works.

	Energy density (Wh/k)	Capacity (Ah)	Life	Electrolyte Injection (g/Ah)	cathode/ Areal loading (mg cm^{-2})	areal capacity (mAh cm^{-2})	N/P	Cell type	Reference ID
This work	**356**	**2.62**	**100**	**3.0**	**NCM811/ 20.0**	**3.80**	**2.11**	**Pouch cell**	
Ref.1	294	0.196	200	-	NCM811/ 22.48	4.1	7.9	Pouch cell	Science Advances 2019, 5 (10). eaax5587
Ref.2	300	1	160	2.7	NCM523/ 22.0	3.38	2.96	Pouch cell	Adv. Energy Mater. 2020, 10, 1903362
Ref.3	300	2.08	120	-	S/7.0	4.7	-	Pouch cell	Energy Storage Materials 2019, 18, 414-422
Ref.4	371	0.207	150	2.9	NCM811/ 21.8	3.93	1.45 5	Pouch cell	Energy Storage Materials 2020, 26, 73-82
Ref.5	340	3.5	60	2.3	NCM523/ 25.5	4.46	1.6	Pouch cell	Angewandte Chemie 2020, 59 (8), 3252-3257
Ref.6	405	0.1	200	-	LiFMP/-	-	-	solid-state lithium batterie	Nano Energy 2016, 28, 447-454

Table S2. The comparisons on Li metal composite anode with different conductive materials prepared by melting/infusion or electrochemical deposition methods and characterized in coin cells or pouch cells.

	Material selection	**Preparation method**	**Controllable lithium content**	**Scalable fabrication**	**Cathode/ Areal loading**	**Cycle life (cycle number-retention)**	**Cell type**	**Reference ID**
Ref.7	carbon fibers	rolling method	×	-	S/ 1.7 mg cm^{-2}	100-98%	Pouch Cell	Advanced Materials 2019, 31 (8), e1807131
Ref.8	carbon felt	thermal infusion	×	×	S/ 2.45 mg cm^{-2}	400-63.8%	Coin cell	Nano Energy 2019, 60, 257-266
Ref.9	carbon paper	electrodeposited	√	×	$LiNi_{0.8}Co_{0.15}Al_{0.05}O_2$/ 4.0-5.0 mg cm^{-2}	200-82.5%	Coin cell	ACS Appl Mater Interfaces 2018, 10 (41), 35296-35305
Ref.10	hollow carbon fiber	electrodeposited	√	×	$LiFePO_4$ / 13.0 mg cm^{-2}	200-91.3%	Coin cell	Joule 2017, 1 (3), 563-575
Ref.11	carbon fibers	thermal infusion	×	×	S/ 1.7 mg cm^{-2}	400-64.3%	Coin cell	Joule 2018, 2 (4), 764-777
Ref.12	Cu mesh	melt infusion	×	×	$LiFePO_4$/ 2.0 mg cm^{-2}	1000-77.6%	Coin cell	Journal of Materials Chemistry A 2019, 7 (10), 5726-5732
Ref.13	Cu mesh	mechanical pressure	×	-	LTO/ -	500-79.7%	Coin cell	Adv. Funct. Mater. 2017, 27, 1606422
This work	**graphene**	**Thermal-initiated Conversion**	√	√	**NCM811/ 20.0 mg cm^{-2}**	**100-75%**	**Pouch cell**	

Table S3. Detailed parameters of the pouch cell.

Components	Value (g)
Li@G anodes	1.788
NCM811 cathodes	14.526
Separator	1.872
Tabs	0.6
Electrolyte	7.8
Al-plastic film	1.2
Total	**27.786**
Capacity	**2.62 Ah**
Average voltage	**3.8 V**
Energy density	**356 Wh/kg**